Electrocatalytic Ammonia Oxidation by a Low Coordinate Copper Complex

Md Estak Ahmed,[†,‡] Mahdi Raghibi Boroujeni,[‡] Pokhraj Ghosh,[†,‡] Christine Greene,[‡] Subrata Kundu,[‡,§] Jeffery A. Bertke,[‡] Timothy H. Warren*[,†,‡]

[†]Department of Chemistry, Michigan State University, East Lansing, MI 48824, United States

[‡]Department of Chemistry, Georgetown University, Box 51277-1227, Washington, D.C. 20057, United States

[§]School of Chemistry, Indian Institute of Science Education and Research Thiruvananthapuram, Kerala 695551, India

KEYWORDS Ammonia oxidation, Earth abundant catalysis, Electrocatalysis, N–N Bond Formation, Mechanism

ABSTRACT: Molecular catalysts for ammonia oxidation to dinitrogen represent enabling components to utilize ammonia as a fuel and/or source of hydrogen. Ammonia oxidation requires not only the breaking of multiple strong N–H bonds, but also controlled N–N bond formation. We report a novel β-diketiminato copper complex [^{t}Pr$_2$NN$_{F6}$]Cu^{I}-NH$_3$ ([Cu^{I}]-NH$_3$ (**2**)) as a robust electrocatalyst for NH$_3$ oxidation in acetonitrile under homogeneous conditions. Complex **2** operates at a moderate overpotential (η = 700 mV) with a TOF$_{max}$ = 940 h^{-1} as determined from CV data in 1.3 M NH$_3$ MeCN solvent. Prolonged (>5 h) controlled potential electrolysis (CPE) reveals the stability and robustness of the catalyst under electrocatalytic conditions. Detailed mechanistic investigations indicate that electrochemical oxidation of [Cu^{I}]-NH$_3$ forms {[Cu^{II}]-NH$_3$}$^+$ (**4**) which undergoes deprotonation by excess NH$_3$ to form reactive copper(II)-amide [Cu^{II}]-NH$_2$ (**6**) unstable towards N–N bond formation to give the dinuclear hydrazine complex [Cu^{I}]$_2$(μ-N$_2$H$_4$). Electrochemical studies reveal that the bisammine complex [Cu^{I}](NH$_3$)$_2$ (**7**) forms at high ammonia concentration as part of the {[Cu^{II}](NH$_3$)$_2$}$^+$/[Cu^{I}](NH$_3$)$_2$ redox couple that is electrocatalytically inactive. DFT analysis reveals a much higher thermodynamic barrier for deprotonation of {[Cu^{II}](NH$_3$)$_2$}$^+$ (**8**) by NH$_3$ to give the four-coordinate copper(II) amide [Cu^{II}](NH$_2$)(NH$_3$) (**9**) (ΔG = 31.7 kcal/mol) as compared to deprotonation of the three coordinate {[Cu^{II}]-NH$_3$}$^+$ by NH$_3$ to provide the reactive three coordinate parent amide [Cu^{II}]-NH$_2$ (ΔG = 18.1 kcal/mol) susceptible to N–N coupling to form [Cu^{I}]$_2$(μ-N$_2$H$_4$) (ΔG = –11.8 kcal/mol).

Introduction

Due to its high energy density and established commercial sources of production and distribution networks, ammonia (NH$_3$) is an especially appealing energy carrier.[1-3] On a per-hydrogen atom basis, ammonia possesses approximately the same energy content as molecular hydrogen. Ammonia can be used directly in fuel cells through the ammonia oxidation reaction (AOR) or can be used as a hydrogen (H$_2$) vector resulting from its high energy density.[4-8] Examples of homogeneous catalysts are attracting increasing attention.[9-16] Homogeneous catalysts offer synthetic control over steric and electronic properties of the active site along with a suite of molecular tools to understand the fundamental chemistry involved through detailed structural, spectroscopic and mechanistic studies.[7]

Ammonia oxidation is a six-electron process that generates nitrogen gas (N$_2$) directly from ammonia. Protons released in the anodic half reaction may be captured by NH$_3$ present in solution with a thermodynamic potential $E°$ = –0.942 mV vs Fc$^{+/0}$

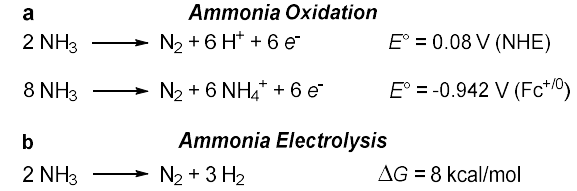

Figure 1. Thermodynamics of ammonia oxidation.

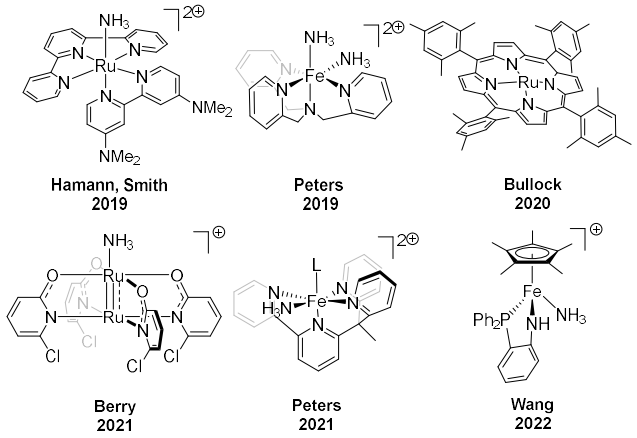

Figure 2. Selected molecular complexes that mediate catalytic ammonia oxidation chemically or electrochemically.

in MeCN, a non-aqueous solvent with relatively high NH$_3$ solubility (Figure 1a). Coupling this anodic reaction with oxygen reduction in MeCN ($E°_{ORR}$ = 0.233 V vs Fc$^{+/0}$) requires a maximum overpotential of +1.18 V to generate useful energy in a direct ammonia fuel cell (DAFC).[16] Alternatively, ammonia electrolysis generates N$_2$ and H$_2$ (Figure 1b), the later for potential use in H$_2$ fuel cells once scrubbed from any remaining ammonia.[17-18]

Ru-based complexes similar to those employed in water oxidation catalysis[19-21] offered an initial blueprint for molecular ammonia oxidation catalysts (Figure 2). Hamann and Smith achieved electrocatalytic ammonia oxidation to N_2 and H_2 using $[Ru(trpy)(dmabpy)(NH_3)][PF_6]_2$ (trpy = 2,2′,2″-terpyridine; dmabpy = 4,4′-bis(dimethylamino)-2,2′-bipyridine) as catalyst.[9, 22] Nishibayashi and co-workers reported ruthenium complexes bearing 2,2′-bipyridyl-6,6′-dicarboxylate ligands work as catalysts for the ammonia oxidation reaction.[13] Llobet and co-workers described the catalytic ammonia oxidation reaction activity using [Ru(tda-κ-N^3O)(py)$_2$], (tda^{2-} is 2,2′:6′,2″-terpyridine-6,6″-dicarboxylate; py is pyridine) as a catalyst precursor.[23] Recently, Berry and co-workers reported the metal-metal bonded mixed-valent $Ru_2(chp)_4OTf$ (chp^- = 6-chloro-2-hydroxypyridinate) that spontaneously forms nitrogen from ammonia without any applied potential. This dinuclear ruthenium species mediates electrocatalytic oxidation of ammonia with an onset potential at −255 mV, generating N_2 and H_2 via controlled potential electrolysis (CPE) at 0.0 V vs $Fc^{0/+}$.[16] Aryloxy radicals ArO• may be used to chemically oxidize ammonia bound to a ruthenium porphyrin complex (porph)Ru(NH_3).[11]

Sustainability considerations motivate the use of earth-abundant transition metals for ammonia oxidation.[12, 14-15, 24] Peters and co-workers have recently described two Fe based electrocatalysts, $[(bpyPy_2Me)Fe(MeCN)_2]^{2+}$ and $[(TPA)Fe(NH_3)_2]OTf_2$ that show efficient ammonia oxidation.[12, 14] The $[(bpyPy_2Me)Fe(MeCN)_2]^{2+}$ catalyst shows the highest turnover number (TON = 149), yet requires significant overpotential (~1.8 V). Very recently, Liao, Ye, Wang and co-workers reported a ferric ammine complex $[Cp^*Fe(1,2\text{-}Ph_2PC_6H_4NH)(NH_3)]^+$ that oxidizes ammonia to N_2 and H_2 electrocatalytically under homogeneous conditions with an overpotential of 770 mV. The redox non-innocent nature of the phenylamido ligand facilitates the concerted transfer of one proton and two electrons.[15]

N–N bond formation represents a key step in ammonia oxidation en route to N_2 formation. Mechanistic data on current homogeneous systems for ammonia oxidation suggest that N–N bond formation may occur after 3-, 2-, or 1-electron oxidation of a metal-ammine complex $[M^n]$-NH_3 (Scheme 1). Three electron oxidation to a metal nitride [M]≡N can result in direct formation of metal-bound N_2 [M]-N_2-[M] through bimolecular coupling (Scheme 1).[7, 25-26] Alternatively, two- or one-electron oxidation can generate electrophilic metal-imide [M]=NH or metal-amide species [M]-NH_2, respectively, susceptible to nucleophilic attack by NH_3 to ultimately form a metal-bound hydrazine ligand in [M]-NH_2NH_2.[9, 27] Although not catalytic, a recent stoichiometric report of a nickel-amide complex $[Ni^{III}]$-NH_2 revealed bimolecular N–N coupling to give the corresponding dinuclear $[Ni^{II}]_2(\mu\text{-}N_2H_4)$ complex.[28]

Scheme 1. Pathways for N–N bond formation in ammonia oxidation.

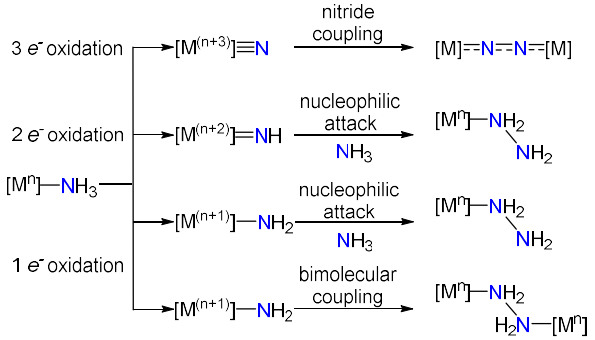

Scheme 2. N–N bond formation promoted by copper β-diketiminate complexes.

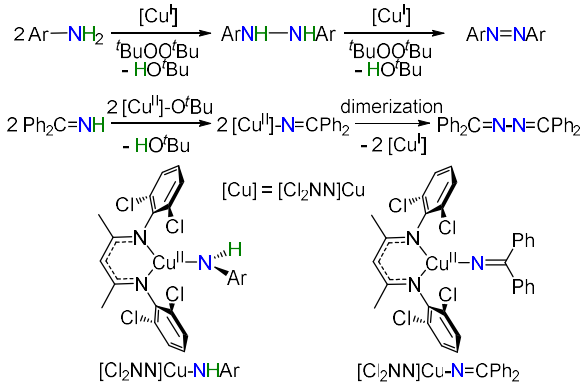

Copper(II) anilide and ketimide intermediates in N-N coupling

Based on the longstanding oxidation of anilines $ArNH_2$ to diazenes ArN=NAr facilitated by copper(I) complexes,[29-30] we explore the use of copper catalysts for ammonia oxidation. Previous mechanistic studies suggest that β-diketiminato copper(II) $[Cu^{II}]$-NHAr species engage in bimolecular coupling to form hydrazines ArNH-NHAr that are readily oxidized to diazenes ArN=NAr.[29,31] Moreover, related copper(II) ketimides $[Cu^{II}]$-N=CPh_2 undergo bimolecular N–N coupling to Ph_2C=N-N=CPh_2 with reduction of routes to the corresponding copper center to $[Cu^{I}]$.[32] Chemical and electrochemical conversion of HNC=Ph_2 to Ph_2C=N-N=CPh_2 represents a model system for ammonia oxidation to hydrazine.[33-34] These observations motivate the exploration of simple β-diketiminato copper ammine complexes $[Cu^{I}]$-NH_3 and $\{[Cu^{II}]\text{-}NH_3\}^+$ that potentially could generate reactive copper(II) amide intermediates $[Cu^{II}]$-NH_2 susceptible to hydrazine formation via bimolecular N-N coupling. This work describes electrocatalytic ammonia oxidation enabled by three coordinate copper(I) and copper(II) ammine complexes.

Results and Discussion

Synthesis of Three Coordinate Copper(I) Complexes. A solution of the yellow β-diketiminato copper(I) complex $[^iPr_2NN_{F6}]Cu(\eta^2\text{-benzene})$[35] turns orange-red upon dissolution in acetonitrile to form $[^iPr_2NN_{F6}]$Cu-NCMe ($[Cu^{I}]$-NCMe; **1**)

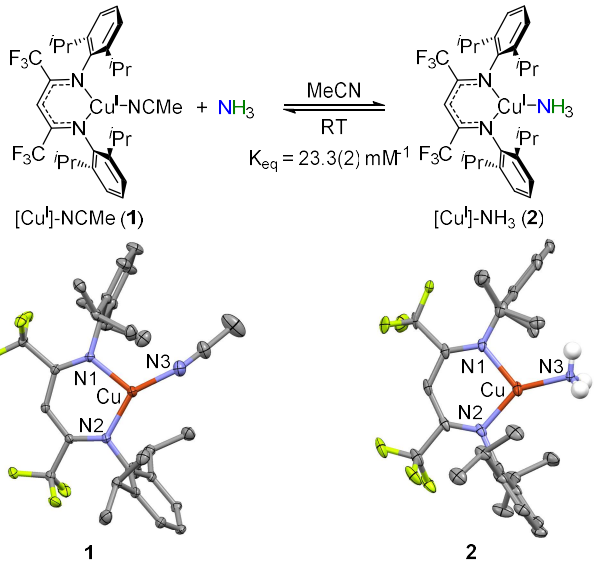

Figure 3. Reversible binding of NH_3 to $[Cu^{I}]$ in MeCN and X-ray structures of $[Cu^{I}]$-NCMe (**1**) and $[Cu^{I}]$-NH_3 (**2**).

isolated in 88% yield. Addition of excess anhydrous ammonia to a solution of **1** in fluorobenzene enables the isolation of [^{i}Pr$_2$NN$_{F6}$]Cu-NH$_3$ ([Cu^{I}]-NH$_3$; **2**) via crystallization at –40 °C in 80% yield.

The X-ray structures of **1** and **2** reveal trigonal-planar geometry at the Cu(I) center with Σ(angles about Cu) = 357.70(9) and 359.96(8)°, respectively, for **1** and **2**. The Cu–N bond distance in [Cu^{I}]-NH$_3$ of 1.905(9) Å is quite similar to the C–N distance in [Cu^{I}]-NCMe of 1.891(4) Å despite the difference in hybridization at N (sp^3 vs sp). There is modest asymmetry in the N1-Cu-L and N2-Cu-L angles (L = MeCN: 109.1(2) and 150.5(2)°; L = NH$_3$: 116.2(3) and 144.5(3)°).

^{1}H NMR spectra of **1** and **2** in CD$_3$CN each show a diagnostic singlet at δ5.54 ppm for the β-diketiminato C–H methine resonance (Figures S1 & S5). ^{1}H NMR spectra of [Cu^{I}]-NH$_3$ in CD$_3$CN, however, possess signals at both δ2.14 and 0.63 ppm corresponding to both bound and free NH$_3$. In the absence of [Cu^{I}], free NH$_3$ (0.6 mM) in CD$_3$CN appears as a broad signal at δ 0.42 ppm (Figure S11). Addition of excess NH$_3$ to **2** in CD$_3$CN results in an increase in the intensity of the signal initially at δ 2.14 ppm that also gently shifts downfield while the broad signal initially at δ 0.63 ppm increases in intensity and shifts upfield toward free NH$_3$ in the absence of the copper(I) β-diketiminate [Cu^{I}]. The observations are consistent with an equilibrium between [Cu^{I}]-NCMe (**1**) and [Cu^{I}]-NH$_3$ (**2**), ultimately favoring **2** at higher ammonia concentrations (Figure 3). At room temperature in MeCN, the equilibrium constant K_{eq} = [**2**]/[**1**][NH$_3$] is 23.3(2) mM^{-1}. IR spectroscopy of [Cu^{I}]-NH$_3$ (**2**) in fluorobenzene reveals a ν(N–H) band at 3370 while [Cu^{I}]-ND$_3$ (**2^{D3}**) possesses a ν(N–D) band at 2508 cm^{-1} (Figures S8 & S9). Each of these bands appear at lower energy relative to free NH$_3$ and ND$_3$ in fluorobenzene at 3409 and 2543 cm^{-1}, respectively (Figure S10).

Electrochemical Investigation of [Cu^{I}]–NCMe (1) and [Cu^{I}]–NH$_3$ (2) Complexes. Cyclic voltammetry studies using a glassy carbon (GC) working electrode in CH$_3$CN with 0.1 M n-tetrabutylammonium hexafluorophosphate ([Bu$_4$N]PF$_6$) as electrolyte shows a redox process for complex **1** centered at 0.225 V vs Fc$^{+/0}$ which we attribute to the Cu$^{II/I}$ redox couple (Figure 4a).[36] The nearly identical oxidation and reduction currents ($I_{p,c}/I_{p,a} \approx 1$) invariant of scan rate illustrates that this couple is essentially fully reversible under these conditions; the peak-to-peak separation ΔE = 72 mV shows near-Nernstian behavior. The peak current (I_p) increases as the square root of the scan rate consistent with a well-behaved, homogeneous redox couple in solution. The electrochemical diffusion coefficient of 4.1 × 10^{-6} cm^{2}s^{-1} comes from application of the Randles-Sevcik equation (Figure S26).

On the other hand, cyclic voltammetry of [Cu^{I}]-NH$_3$ (**2**) in CH$_3$CN shows an irreversible redox event at 0.07 V vs Fc$^{+/0}$ (Figure 4b). The large peak-to-peak separation (ΔE = 300 mV) and $I_{p,a} > I_{p,c}$ values suggest electron transfer followed by a chemical reaction (EC process).[37] Addition of 10 equiv. NH$_3$ to complex **2** further cathodically shifts $E_{1/2}$ by 160 mV to –0.08 V; addition of a large excess NH$_3$ (~ 200 equiv.) results in an irreversible faradaic process with loss of the cathodic wave ($I_{p,a} >> I_{p,c}$). These observations suggest an electrocatalytic process that depends on the concentration of NH$_3$.[37]

Electrochemical Ammonia Oxidation. To gain insight into the mechanism responsible for electrocatalysis, we investigated the CV response as a function of the concentration of both the copper(I) β-diketiminate catalyst [Cu^{I}] as well as ammonia. Varying the catalyst concentration over the range 0.09 – 1.22 mM, the catalytic current (I_{cat}) increases linearly under conditions of constant ammonia concentration ([NH$_3$] = 1.3 M) (Figure 5a). Thus, the reaction is first order in [catalyst] that exists as [Cu^{I}]-NH$_3$ (**2**) under conditions employed for electrocatalysis. Holding the catalyst concentration constant ([Cu] = 1.0 mM), varying the ammonia concentration over the range 0.55 – 1.30 M results in I_{cat} values that increase as the square-root of [NH$_3$]. Following the relationship that relates I_{cat} with [substrate] (Figure 5b, inset),[38] the electrocatalytic process is also first order in [NH$_3$] (Figure 5b). Thus, we arrive at the rate law: rate = k_{NH3}[Cu^{I}-NH$_3$][NH$_3$]. At an ammonia concentration of 1.3 M, the TOF_{max} determined from the catalytic response obtained at various scan rates[39] is 0.26(1)s^{-1} or ca. 940 h^{-1} (Figure 5c) leading to k_{NH3} = 0.2 M^{-1}s^{-1}. Electrocatalysis with varying concentrations of ND$_3$ led to a linear response of I_{cat} vs [ND$_3$]$^{1/2}$, yet one shallower than I_{cat} vs [NH$_3$]$^{1/2}$ corresponding to a primary kinetic isotope effect k_H/k_D of 2.4(2) (Figure 5d). In electrocatalysis of 1.3 M NH$_3$ with 1.0 mM [Cu^{I}], we note an onset

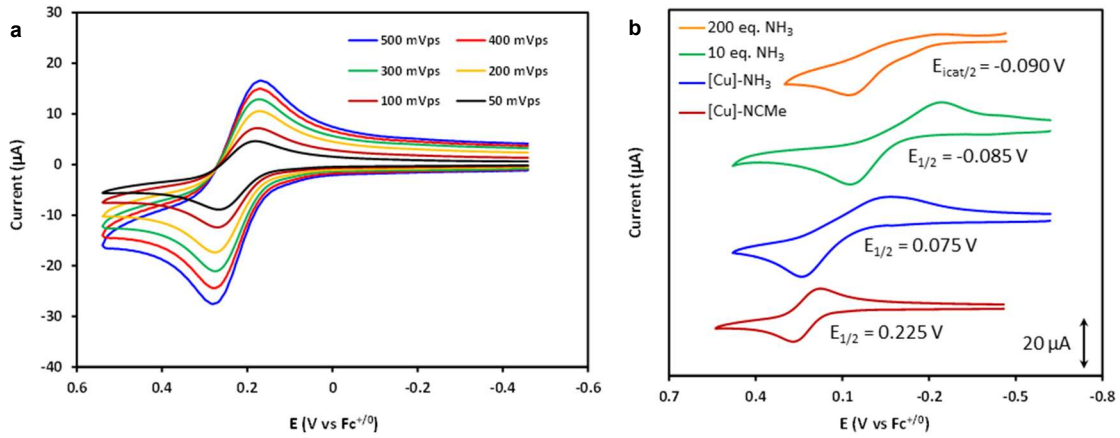

Figure 4. (**a**) Cyclic voltammograms of 1.0 mM [Cu]-NCMe (**1**) in acetonitrile referenced vs Fc$^{+/0}$ at scan rates: 50 – 500 mV/s. (**b**) Cyclic voltammograms in acetonitrile of 1.0 mM [Cu^{I}]-NCMe (**1**) (maroon) as well as 1.8 mM [Cu^{I}]-NH$_3$ (**2**) (blue) in the presence of 10 equiv. NH$_3$ (green) and 200 equiv. NH$_3$ (orange): scan rate: 100 mV/s. Conditions: 100 mM [Bu$_4$N]PF$_6$ supporting electrolyte with GC working, Pt counter and Ag/AgNO$_3$ reference electrodes.

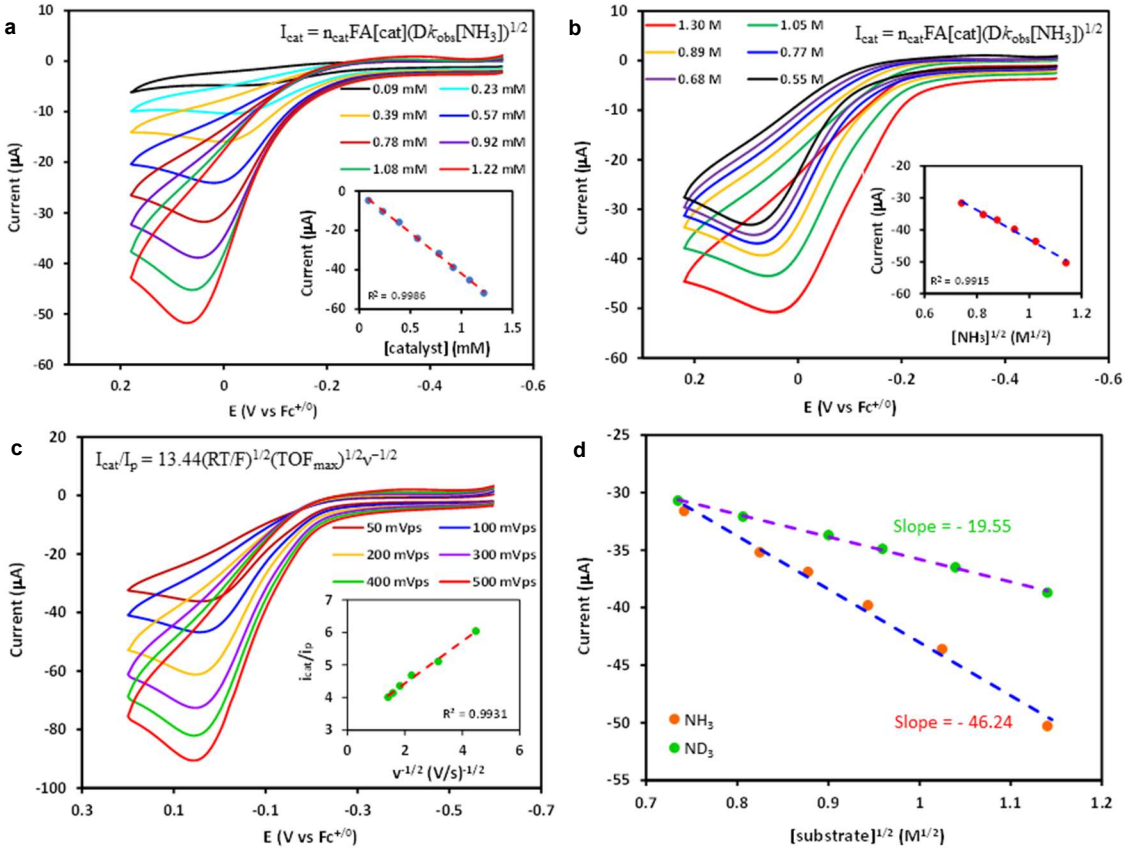

Figure 5. Electrocatalytic ammonia oxidation. (**a**) Cyclic voltammograms of 0.09 – 1.22 mM [Cu^{I}]-NCMe (**1**) in 1.3 M NH_3 in acetonitrile; scan rate: 100 mV/s. (**b**) Cyclic voltammograms of 1.0 mM [Cu]-NCMe in acetonitrile containing 0.55 – 1.3 M NH_3; scan rate: 100 mV/s. (**c**) Cyclic voltammograms of 1.0 mM [Cu]-NCMe in acetonitrile containing 1.3 M NH_3 at scan rates of 50 – 500 mV/s. (inset) I_{cat}/I_p vs $v^{-1/2}$ plot. (**d**) Plots of catalytic peak current vs [substrate]$^{1/2}$ to determine k_H/k_D. Conditions: 100 mM $[Bu_4N]PF_6$ supporting electrolyte with GC working, Pt counter and $Ag/AgNO_3$ reference electrodes.

potential of –0.24 V corresponding to a modest onset overpotential $\eta = 0.70$ V.

Controlled Potential Electrolysis and Product Analysis. Controlled potential electrolysis (CPE) of a 1.3 M NH_3 solution in MeCN at 0.0 V vs $Fc^{+/0}$ by [Cu^{I}]-NH_3 (**2**) (1.0 mM) generates N_2 and H_2 (Figures 6 and S35). CPE performed using a 2 cm^2 glassy carbon working electrode with Pt mesh and $Ag/AgNO_3$ as counter and reference electrodes, respectively. Headspace gas analysis of the CPE cell by gas chromatography revealed N_2 and H_2 in the molar ratio of 1:2.64. This corresponds to a faradaic efficiency (FY) of 84% for N_2 evolution (Figure S34) as well as a TON of 6.2 after 3 h. A separate experiment under identical conditions produces the same current (0.98 mA) sustained for at least 5 h (Figure 6).

The sustained CPE currents in 1.3 M NH_3 MeCN solutions result from ammonia oxidation by the homogeneous [Cu^{I}] catalyst. There is minimal background current in the absence of the copper(I) β-diketiminate complex (Figure 6, red trace). After carrying out CPE for 2 h, the glassy carbon electrode alone after rinsing showed no electrocatalytic current in the absence of added [Cu^{I}] catalyst (Figure S32). Moreover, the copper catalyst appears quite stable under CPE conditions. UV-vis spectroscopy before and after CPE experiment (3 h) showed minimal (~8%) catalyst degradation with respect to its initial concentration (Figure S36).

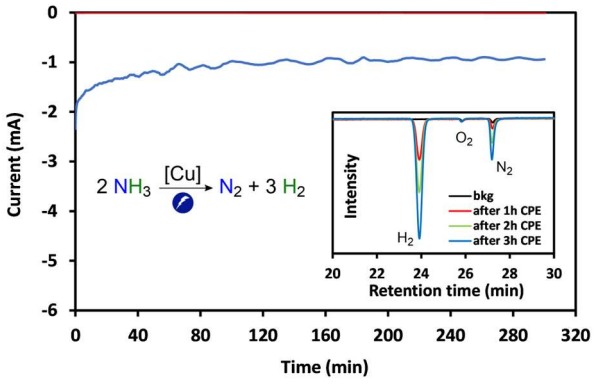

Figure 6. Long-term controlled potential electrolysis of [Cu] catalyst. Chronoamperometric measurement at 0.0 V vs $Fc^{+/0}$ of 1.3 M NH_3 in acetonitrile (1.0 mM [Cu^{I}], blue line; no catalyst, red line). Gas chromatograms illustrating increasing N_2 and H_2 in the electrochemical cell headspace with increasing time (inset).

Synthetic and Mechanistic Studies: Intermediates in Ammonia Oxidation. To gain insight into the discrete copper complexes responsible for the electrocatalytic oxidation of ammonia, we sought to outline the chemical reactivity of likely copper(II) intermediates (Scheme 3). One electron oxidation of [Cu^{I}]-NCMe (**1**) by $AgPF_6$ in fluorobenzene (PhF) produced a stable purple salt assigned as {[Cu^{II}](PhF)}PF_6 (**3-PhF**) that converts to {[Cu^{II}](THF)}PF_6 (**3-THF**) when crystallized from a THF/pentane mixture at –40 °C. While we were unable to determine the X-ray structure of the fluorobenzene adduct **3-PhF**, the X-ray structure of **3-THF** displays a three-coordinate copper(II) center with short Cu–N1, Cu–N2, and Cu–O distances of 1.860(6), 1.874(5), and 1.923(5) Å, respectively (Figure 7). The EPR spectrum of **3-THF** shows an axial pattern simulated with $g_{\parallel} = 2.400$ and $g_{\perp} = 2.091$ that exhibits clearly resolved hyperfine $A_{\parallel}(^{63/65}Cu) = 400$ MHz from the low field component (Figure S17).

Careful addition of just less than 1 equiv. NH_3 to {[Cu^{II}](PhF)}PF_6 (**3-PhF**) in fluorobenzene at –40 °C enabled crystallization of thermally unstable {[Cu^{II}]-NH_3}PF_6 (**4**) (Scheme 3ii). X-ray characterization of **4** reveals a three coordinate, T-shaped monoammine complex with dramatically different $N_{\beta\text{-dik}}$-Cu-N_{ammine} angles of 107.2(4) and 157.2(1)° (Figure 7). The Cu-N_{ammine} distance of 1.905(9) Å in cationic **4** is contracted compared to 1.936(9) Å in neutral Cu(I) analogue **2**. Frozen glass EPR spectra in fluorobenzene reveal an axially biased spectrum simulated with $g_z = 2.200$, $g_y = 2.060$, and $g_x = 2.050$ along with a large copper hyperfine $A_z(^{63/65}Cu) = 518$ MHz from the low field component (Figure S18). Cyclic voltammetry of a solution of **4** in acetonitrile gives similar waves as [Cu^{I}]-NH_3 (**2**) (Figures 4b and S19).

Anticipating hydrazine (N_2H_4) as a possible direct oxidation product of NH_3, we added hydrazine to the copper(I) β-diketminato catalyst [Cu^{I}] in fluorobenzene (Scheme 3iii). The dinuclear {[^{i}Pr$_2$NN$_{F6}$]Cu}$_2$(μ-N_2H_4) ([Cu^{I}]$_2$(μ-N_2H_4), **5**) forms, isolated as red crystals in 86% yield. The X-ray structure of **5** possesses an inversion center that relates the two β-diketiminato copper fragments with distances Cu–N3 1.984(2) and N3-N3′ 1.497(2) Å for the bound hydrazine (Figure 7). ^{1}H NMR spectroscopy of **5** in CD_3CN exhibits a singlet at δ 2.09 ppm due to coordinated N_2H_4 along with a diagnostic signal for the β-diketiminate backbone C–H methine at δ 5.55 ppm (Figure S13). The ^{19}F NMR spectrum of **5** shows a sharp peak at δ 63.64 ppm (Figure S15).

The cationic monoammine complex {[Cu^{II}]-NH_3}PF_6 (**4**) is unstable in the presence of added base. Addition of a slight excess of NH_3 (4 equiv.) to **4** in fluorobenzene at –40 °C forms red [Cu^{I}]$_2$(μ-N_2H_4) (**5**) along with the free β-diketiminato ligand H[^{i}Pr$_2$NN$_{F6}$] in a 2:1 ratio as analyzed by ^{1}H NMR (Scheme 3iv-3v and Figure S20). We hypothesize that NH_4^+ formed as a result of deprotonation of the ammine ligand in {[Cu^{II}]-NH_3}$^+$ by added NH_3 leads to an acid-base reaction between NH_4^+ and the anionic β-diketiminate ligand in [Cu^{I}]-NCMe. Accordingly, addition of 1 equiv. [NH_4]PF_6 to [Cu^{I}]-NCMe in CD_3CN forms the free β-diketimine ligand H[^{i}Pr$_2$NN$_{F6}$] in 33% yield (Figure S24).

We then examined the reaction of {[Cu^{II}]-NH_3)}PF_6 (**4**) with DBU, a strong, non-nucleophilic base whose conjugate acid [H-DBU]$^+$ (pK_a = 24.3 in MeCN) is much less acidic than NH_4^+ (pKa = 16.5 in MeCN). Addition of 4 equiv. DBU to **4** in PhF results in [Cu^{I}]$_2$(μ-N_2H_4) (**5**) along with a small amount of H[^{i}Pr$_2$NN$_{F6}$] in 4:1 ratio as observed in ^{19}F NMR spectroscopy (Scheme 3vi and Figure S21). Thus, the cationic monoammine complex {[Cu^{II}]-NH_3}PF_6 (**4**) undergoes ready deprotonation to ultimately form the dinuclear copper(I) hydrazine complex [Cu^{I}]$_2$(μ-N_2H_4) (**5**).

To provide evidence for the anticipated copper(II) amido intermediate [Cu^{II}]-NH_2 (**6**) that we hypothesize dimerizes to

Scheme 3. Synthetic investigation of key copper complexes in ammonia oxidation. (i) Oxidation of [Cu^{I}]-NCMe (**1**) by $AgPF_6$ to give {[Cu^{II}](PhF)}$^+$ (**3-PhF**); (ii) reaction of **3-PhF** with NH_3 to form {[Cu^{II}]-NH_3}$^+$ (**4**); (iii) addition of N_2H_4 to **1** to form [Cu^{I}]$_2$(μ-N_2H_4) (**5**); (iv) formation of [Cu^{II}]-NH_2 (**6**) via deprotonation of **4**; (v) dimerization of [Cu^{II}]-NH_2 to [Cu^{I}]$_2$(μ-N_2H_4); (vi) deprotonation of **4** to give **5**; (vii) reaction of trityl radical with **6** to give Ph_3C–NH_2: (viii) displacement of N_2H_4 from **5** with excess NH_3 to give **2**.

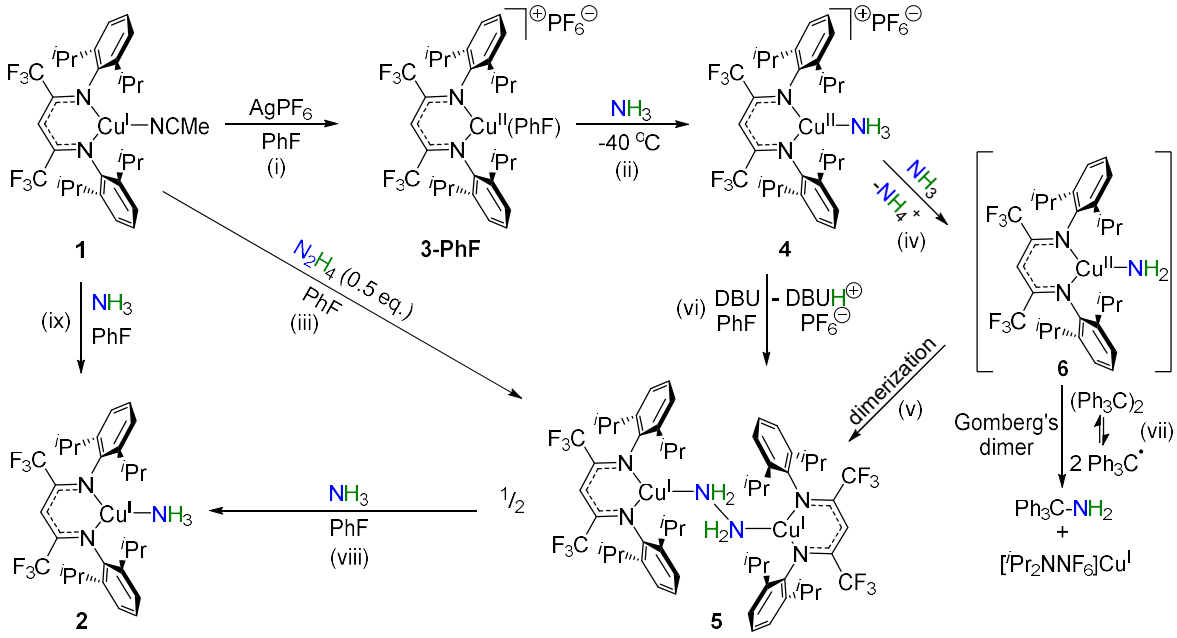

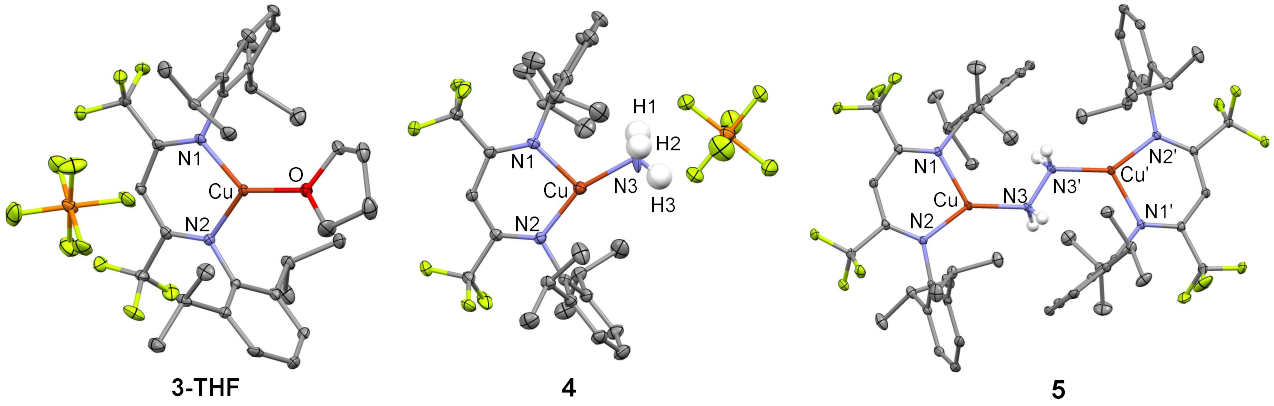

Figure 7. X-ray structures of copper complexes {[Cu^{II}]-THF}PF$_6$ (3-THF), {[Cu^{II}]-NH$_3$}PF$_6$ (4), and [Cu^{I}]$_2$(μ-N$_2$H$_4$) (5). Thermal ellipsoids are shown at 50% probability. All hydrogen atoms bound to carbon are omitted for clarity.

form [Cu^{I}]$_2$(μ-N$_2$H$_4$) (**5**) (Scheme 3v), we considered chemical probes to trap the reactive amido functionality in [Cu^{II}]-NH$_2$. Along with many β-diketiminato copper(II) complexes [Cu^{II}]-X that react with radicals R• to form R–X,[29-31, 36] the copper(II) anilide [Cl$_2$NN]Cu-NH(2-py) undergoes reaction with Gomberg's dimer that generates a small equilibrium amount of the trityl radical (Ph$_3$C•) to provide Ph$_3$C-NH(2-py) in 78% yield.[31] Anticipating formation of [Cu^{II}]-NH$_2$ via deprotonation of {[Cu^{II}]-NH$_3$}PF$_6$ (**4**) in the presence of excess NH$_3$, carrying out this reaction in acetone-d_6 with Gomberg's dimer gives Ph$_3$C–NH$_2$ in 32% yield (Scheme 3iv and 3vii). Importantly, a control experiment between Gomberg's dimer and excess NH$_3$ in absence of {[Cu^{II}]-NH$_3$}PF$_6$ (**4**) does not show the formation of Ph$_3$C–NH$_2$.

Fate of Hydrazine. Synthetic studies show that the addition of excess ammonia (200 equiv.) to [Cu^{I}]$_2$(μ-N$_2$H$_4$) (**5**) results in loss of hydrazine to give [Cu^{I}]-NH$_3$ (**2**) (Scheme 3viii and Figure S25). Thus, under electrocatalytic conditions that employ excess NH$_3$, free hydrazine will form from {[Cu^{II}]-NH$_3$}$^+$ (**4**) via the dinuclear hydrazine complex [Cu^{I}]$_2$(μ-N$_2$H$_4$) (**5**).

Free hydrazine undergoes oxidation at the bare glassy carbon electrode with an onset potential of –0.40 V vs Fc$^{+/0}$ (Figure S37a). Since electrocatalytic ammonia oxidation by [^{i}Pr$_2$NN$_{F6}$]Cu occurs at potentials –0.24 V and higher, any hydrazine produced via ammonia oxidation electrocatalysis would be rapidly oxidized by the glassy carbon working electrode. Nonetheless, we investigated the cyclic voltammetry of [Cu^{I}]$_2$(μ-N$_2$H$_4$) (**5**) that shows evidence of a quasi-reversible wave centered at 0.21 V vs Fc$^{+/0}$. Additionally, there is evidence of an irreversible oxidation feature at ca. 0.1 V that corresponds to the oxidation of free hydrazine (Figure S37c) confirmed through cyclic voltammograms of hydrazine (1 – 10 mM) in the presence of [Cu^{I}] (2.0 mM) (Figure S37b).

Electrocatalytic Ammonia Oxidation: Catalytic Cycle. The combination of electrochemical and mechanistic studies allows us to describe an overall catalytic cycle for ammonia electrooxidation by the copper(I) β-diketiminato catalyst [^{i}Pr$_2$NN$_{F6}$]Cu in acetonitrile (Figure 8). In the presence of excess NH$_3$ (typically 1.3 M NH$_3$), the copper β-diketiminato catalyst [^{i}Pr$_2$NN$_{F6}$]Cu rests as [Cu^{I}]-NH$_3$ (**2**). Oxidation at the anode produces cationic {[Cu^{II}]-NH$_3$}$^+$ (**3**) that undergoes turnover limiting deprotonation by excess NH$_3$ to give [Cu^{II}]-NH$_2$,

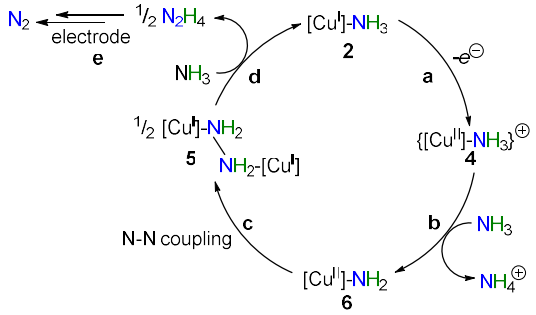

Figure 8. Proposed catalytic cycle for electrocatalytic NH$_3$ oxidation via [Cu^{I}]-NH$_3$ (**2**).

consistent with the electrochemical rate law (rate = k[Cu^{I}-NH$_3$][NH$_3$]). The copper(II) amide [Cu^{II}]-NH$_2$ undergoes rapid N–N bond formation to give [Cu^{I}]$_2$(μ-N$_2$H$_4$) that releases hydrazine upon displacement by excess NH$_3$ (Figure S25). Oxidation of free N$_2$H$_4$ occurs at the anode to give N$_2$. Under CPE conditions that employ an open cell, we anticipate that reduction of NH$_4^+$ occurs to generate H$_2$ at the counter electrode to complete the cell circuit.

Low Potential Reversible Redox Process. [^{i}Pr$_2$NN$_{F6}$]Cu exhibits a reversible redox feature in MeCN at a potential below –0.4 V vs Fc$^{+/0}$ in reasonably concentrated NH$_3$ solutions. Both the current and the potential for this redox event depend on the concentration of NH$_3$. As [NH$_3$] increases from 0.60 to 1.3 M, CV of a 1.0 mM solution of [^{i}Pr$_2$NN$_{F6}$]Cu using a 0.07 cm^2 GC electrode with a scan rate of 100 mV/s results in an increase in the current from 1.8 to 4.8 μA while $E_{1/2}$ becomes more cathodic, shifting from –0.44 to –0.60 V (vs Fc$^{+/0}$) (Figure 9a). These observations are consistent with the formation of a bisammine complex.

[Cu^{I}](NH$_3$)$_2$ (**7**) undergoes essentially reversible oxidation to {[Cu^{II}](NH$_3$)$_2$}$^+$ (**8**) at a much lower potential than the monoammine complex [Cu^{I}]-NH$_3$ (**2**) (E_{ox} = –0.1 V) due to the electron-rich nature of the bisammine complex (Figure 9b). The current increases with increasing [NH$_3$] due to a shift of the equilibrium position towards [Cu^{I}](NH$_3$)$_2$ that increases the concentration of this bisammine complex. Moreover, plotting the $E_{1/2}$ vs log[NH$_3$] reveals a linear relationship that signals binding of NH$_3$ to [Cu^{I}]-NH$_3$ in solution to generate the species involved in the redox event (Figure 9a, inset).[40]

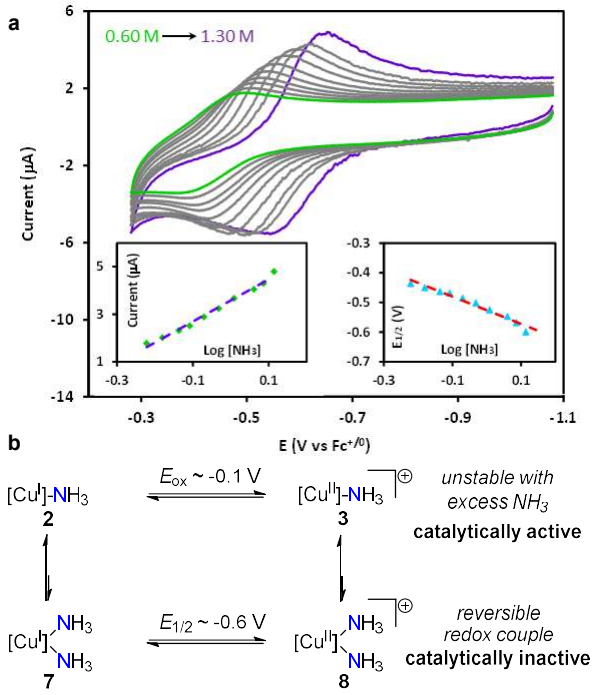

Figure 9. (**a**) Low potential region of CVs taken with 1.0 mM [Cu]-NCMe in acetonitrile with increasing concentration of ammonia; scan rate: 100 mV/s. (inset) $E_{1/2}$ and current intensities change linearly with log [NH_3]. (**b**) Equilibrium between monoamine and bisammine complexes at neutral copper(I) and cationic copper(II) β-diketiminato complexes.

Computational Studies. Recognizing {[Cu^{II}]-NH_3}$^+$ (**4**) as a key intermediate generated upon electrochemical oxidation of [Cu^{I}]-NH_3 (**2**), we examined transformations that cationic **4** may engage in based on electrochemical and synthetic studies employing computational methods at the UBP86+GD3BJ/6-311++G(d,p)/SMD-acetonitrile//BP86/6-311+G(d,p)/gas) level of theory.

Deprotonation of {[Cu^{II}]-NH_3}$^+$ (**4**) by NH_3 to give [Cu^{II}]-NH_2 and NH_4^+ is endergonic by 18.1 kcal/mol. A relaxed energy scan reveals no additional barrier for deprotonation. Considering the presence of excess ammonia, NH_4^+ exists as [NH_4•NH_3]$^+$, 3.1 kcal/mol lower in free energy than NH_4^+ alone. Dimerization of [Cu^{II}]-NH_2 (**6**) via N–N coupling to form [Cu^{I}]$_2$(μ-N_2H_4) (**5**) is exergonic by 11.8 kcal/mol (per Cu center). While displacement of hydrazine from [Cu^{I}]$_2$(μ-N_2H_4) (**5**) to form [Cu^{I}]-NH_3 (**2**) is endergonic by 6.1 kcal/mol, experimental studies show that the presence of a large excess of NH_3 leads to the observation of free N_2H_4 and [Cu^{I}]-NH_3 by ^{1}H NMR spectroscopy (Scheme 3viii and Figure S25).

Binding of NH_3 to {[Cu^{II}]-NH_3}$^+$ (**4**) to form {[Cu^{II}](NH_3)$_2$}$^+$ (**8**) is endergonic by 8.8 kcal/mol, although thermodynamically more favored than deprotonation of **4** by NH_3 to give reactive [Cu^{II}]-NH_2 (**6**) and NH_4^+. Thus, we examined the possibility of deprotonation of {[Cu^{II}](NH_3)$_2$}$^+$ (**8**) to give the four-coordinate amide-ammine complex [Cu^{II}](NH_2)(NH_3) (**9**) which has a thermodynamic barrier of 22.9 kcal/mol (31.7 kcal/mol uphill from {[Cu^{II}]-NH_3}$^+$ + 2 NH_3). The unfavorable thermodynamics for deprotonation to [Cu^{II}](NH_2)(NH_3) (**9**) is consistent with the reversible [Cu^{I}](NH_3)$_2$ / {[Cu^{II}](NH_3)$_2$}$^+$ redox couple observed in the low potential region in cyclic voltammograms of [Cu^{I}] with excess NH_3 (Figure 9). Moreover, the increase in current and cathodic shift of this feature with increasing ammonia concentration (Figure 9a) reflects the endergonicity of NH_3 binding of a second equivalent of NH_3 to [Cu^{I}]-NH_3 and {[Cu^{II}]-NH_3}$^+$, each uphill in free energy by 15.1 and 8.8 kcal/mol, respectively.

Two features account for the dramatically lower thermodynamic barrier for deprotonation of the cationic, three coordinate {[Cu^{II}]-NH_3}$^+$ (**4**) vs. {[Cu^{II}](NH_3)$_2$}$^+$ (**8**). The greater Lewis acidity of the three coordinate center in {[Cu^{II}]-NH_3}$^+$ certainly results in a greater acidity of the ammine N–H bond that primes it for deprotonation as compared to the more electron rich, four coordinate {[Cu^{II}](NH_3)$_2$}$^+$.

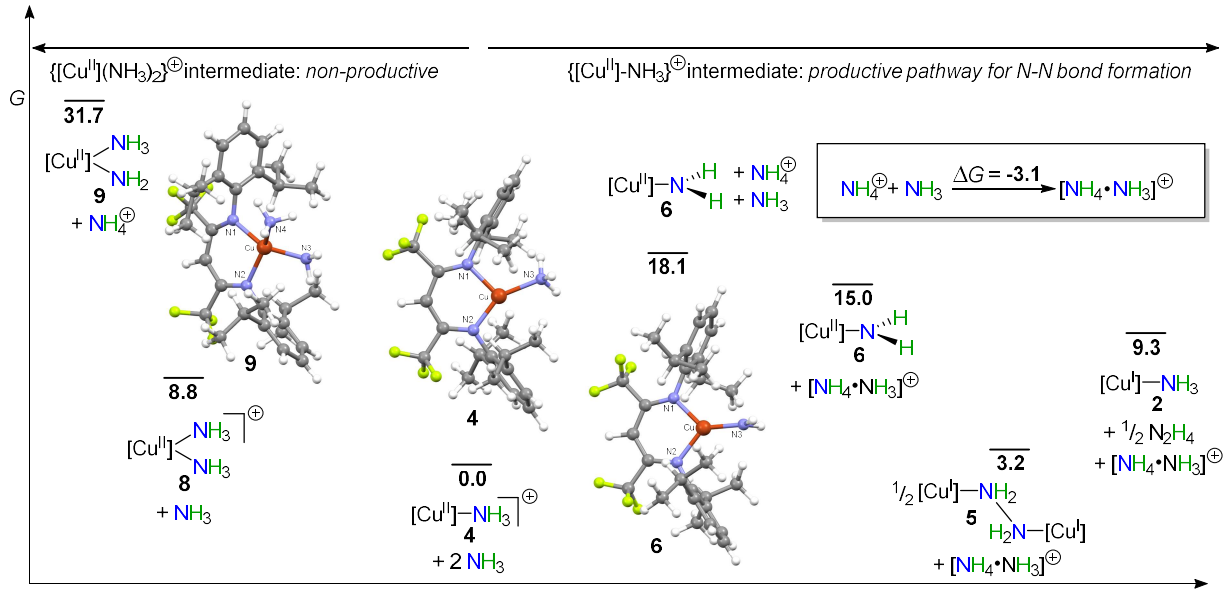

Figure 10. Reaction coordinate diagram for NH_3 oxidation from {[Cu^{II}]-NH_3}$^+$ (**4**). (Right) Productive pathway begins with deprotonation to [Cu^{I}]-NH_2 (**6**) subject to dimerization to [Cu^{I}]$_2$(μ-N_2H_4) (**5**). (Left) Non-productive pathway involves coordination of NH_3 to **4** to give bisammmine complex {[Cu^{II}](NH_3)$_2$}$^+$ (**8**). Free energies (**bold**) in kcal/mol at 298.15 K.

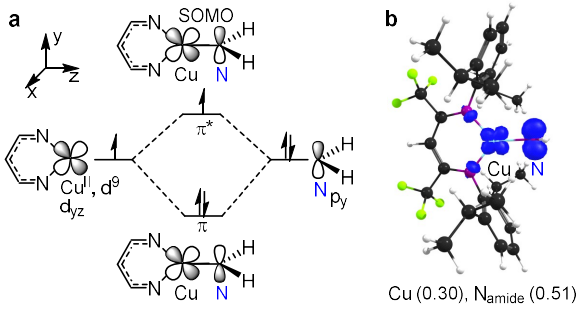

Figure 11. Electronic structure of copper(II) amide **6** illustrating (**a**) Cu-N π-bonding and (**b**) a spin density plot.

The unique electronic structure of the three coordinate $[Cu^{II}]$-NH_2 (**6**) also contributes to the ability of $\{[Cu^{II}]$-$NH_3\}^+$ (**4**) to undergo deprotonation by NH_3. There is a 2-center, 3-electron π-interaction between the highest energy d-orbital of the d^9 Cu^{II} center destabilized by σ-donor interactions with the *β*-diketiminate ligand and the N-lone pair of the sp^2-hybridized amide ligand (Figure 11a). This results in a π-bond order of ½ that strengthens the Cu-N interaction and places considerable unpaired electron density at the amide N atom (0.51 e^-) (Figure 11b). In contrast, there is no empty or half-occupied d orbital in the four-coordinate $[Cu^{II}](NH_2)(NH_3)$ (**9**) positioned to overlap with the amide lone pair, resulting in a longer Cu–NH_2 bond (1.927 Å) and a pyramidalized amide ligand (Σ(angles about N_{amide}) = 335.9°) with somewhat less unpaired electron density on the amide N atom (0.40 e^-) (Figure S47). The significant unpaired electron density at the amide N atom in the three-coordinate $[Cu^{II}]$-NH_2 (**6**) enables facile N–N coupling to form observed $[Cu^I]_2(\mu$-$N_2H_4)$ (**5**).

Conclusions

The *β*-diketiminato copper complex [^{i}Pr$_2$NN]Cu oxidizes ammonia electrocatalytically in acetonitrile medium at a moderate onset overpotential (700 mV) with a TOF_{max} = 940 h^{-1} from CV data in 1.3 M NH_3 in MeCN solvent. This catalyst rests as $[Cu^I]$-NH_3 (**2**) in acetonitrile in the presence of excess NH_3. Electrochemical data reveal that ammonia oxidation is first order in both $[Cu^I]$-NH_3 (**2**) and $[NH_3]$ give the overall rate law: rate = k[Cu-NH_3][NH_3]. A primary KIE of 2.4 observed with ND_3 suggests N–H bond cleavage in or before the turnover-limiting step. Run under controlled potential electrolysis conditions in an open cell, this system exhibits good Faradaic efficiency for N_2 (84%) and H_2 (74%) formation with constant activity for hours in 1.3 M NH_3 in acetonitrile.

Chemical reactivity studies suggest that $[Cu^I]$-NH_3 (**2**) likely forms $\{[Cu^{II}]$-$NH_3\}^+$ (**4**) under electrooxidative conditions, synthetically prepared by addition of less than 1 equiv. NH_3 to copper(II) solvent species $\{[Cu^{II}](PhF)\}^+$ (**3-PhF**). This copper(II) monoammine complex **4** undergoes ready deprotonation by NH_3 to form the hydrazine complex $[Cu^I]_2(\mu$-$N_2H_4)$ (**5**) via the likely intermediacy of copper(II) amide $[Cu^{II}]$-NH_2 (**6**). Displaced by NH_3, the hydrazine ligand in **5** becomes oxidized at the glassy carbon working electrode surface at potential lower than NH_3 at [Cu], leading to N_2 formation.

The low coordination number of three appears critical for facile electrocatalytic oxidation of ammonia to hydrazine. Cyclic voltammetry in ammonia-rich solutions reveals $[Cu^I](NH_3)_2$ / $\{[Cu^{II}](NH_3)_2\}^+$ as a reversible redox couple at low potential (ca. –0.6 V vs $Fc^{+/0}$) that does not participate in electrocatalysis. Instead, the three coordinate $\{[Cu^{II}]$-$NH_3\}^+$ undergoes ready deprotonation by NH_3 to give the trigonal $[Cu^{II}]$-NH_2 (**6**). The Cu-N_{amide} π-bond order of ½ in **6** both facilitates deprotonation as well as places significant electron density at the N_{amide} atom, priming it for N–N coupling with another equivalent of copper(II) amide **6** to give hydrazine complex $[Cu^I]_2(\mu$-$N_2H_4)$ (**5**).

These studies underscore the importance of supporting ligand design to produce three coordinate monoamminecopper(II) complexes $\{[Cu^{II}]$-$NH_3\}^+$ that resist reaction with excess NH_3 to form ubiquitous, stable polyammine species $\{Cu(NH_3)_n\}^{2+}$ (n = 4-6).[41] A testament to their stability, over 400 years ago Andreas Libavius described the deep blue color of the complex now known to be aqueous $[Cu(NH_3)_4]^{2+}$ that results from the action of ammonia in water on bronze (a copper alloy) under aerobic conditions.[42-43]

Future efforts will focus on ancillary ligands that limit the formation of catalytically inactive, four coordinate diammine complexes $\{[Cu^{II}](NH_3)_2\}^+$. Synthetic, electrochemical, and computational investigations suggest turnover-limiting N–H deprotonation of three coordinate $\{[Cu^{II}]$-$NH_3\}^+$ species to give $[Cu^{II}]$-NH_2 susceptible to dimerization to $[Cu^I]_2(\mu$-$N_2H_4)$ that releases hydrazine. In this copper system for electrocatalytic ammonia oxidation, balancing the ease of oxidation of $[Cu^I]$-NH_3 complexes along with ability to deprotonate the resulting $\{[Cu^{II}]$-$NH_3\}^+$ species appear two key factors to control overpotential (*η*) and rate (TOF), respectively.

ASSOCIATED CONTENT

Supporting Information

Experimental and X-ray structure details, DFT calculation details (PDF); X-ray data for **1**, **2**, **3-THF**, **4**, and **5** (CIF).

Accession Codes

CCDC 2150588 and 2165456-215459 contain the supplementary crystallographic data for this paper. These data can be obtained free of charge via www.ccdc.cam.ac.uk/data_request/cif, or by emailing ata_request@ccdc.cam.ac.uk. or by contacting The Cambridge Crystallographic Data Centre, 12 Union Road, Cambridge CB2 1EZ, UK; fax: +44 1223 336033.

AUTHOR INFORMATION

Corresponding Author

Timothy H. Warren – *Department of Chemistry, Michigan State University, East Lansing, MI 48824, United States; Department of Chemistry, Georgetown University, Washington, D.C. 20057, United States;* orcid.org/0000-0001-9217-8890; Email: warre155@msu.edu

Authors

Md Estak Ahmed − *Department of Chemistry, Michigan State University, East Lansing, MI 48824, United States; Department of Chemistry, Georgetown University, Washington, D.C. 20057, United States*; orcid.org/0000-0002-0817-2099

Mahdi Raghibi Boroujeni − *Department of Chemistry, Georgetown University, Washington, D.C. 20057, United States*; orcid.org/0000-0001-8146-5878

Pokhraj Ghosh − *Department of Chemistry, Michigan State University, East Lansing, MI 48824, United States; Department of Chemistry, Georgetown University, Washington, D.C. 20057, United States;* orcid.org/0000-0002-9306-3144

Christine Greene − *Department of Chemistry, Georgetown University, Washington, D.C. 20057, United States*
Subrata Kundu − *School of Chemistry, Indian Institute of Science Education and Research, Thiruvananthapuram, Kerala 695551, India; Department of Chemistry, Georgetown University, Washington, D.C. 20057, United States;* orcid.org/0000-0001-3991-5838
Jeffery A. Bertke − *Department of Chemistry, Georgetown University, Washington, D.C. 20057, United States;* orcid.org/0000-0002-3419-5163

Author Contributions

M.E.A. and M.R.B. contributed equally.

Notes

The authors declare no competing financial interest.

ACKNOWLEDGMENT

THW acknowledges support from the U.S. Department of Energy, Office of Science, Basic Energy Sciences (DE-SC001779). We sincerely acknowledge Prof. John L. McCracken (MSU) for helping us to collect EPR data. We are grateful to Dr. Rui Huang (MSU) for assistance with CHN analyses. We thank Reza Ghazfar (MSU) for assistance with GC-TCD. We thank Dr. Richard Staples (MSU) for assistance with the X-ray structure of compound **1**. Funding for the single-crystal X-ray diffractometer at MSU was provided through the MRI program by the National Science Foundation under Grant No. 1919565.

REFERENCES

1. Erisman, J. W.; Sutton, M. A.; Galloway, J.; Klimont, Z.; Winiwarter, W., How a Century of Ammonia Synthesis Changed the World. *Nat. Geosci.* **2008,** *1*, 636-639.
2. Lan, R.; Tao, S., Ammonia as a Suitable Fuel for Fuel Cells. *Front. Energy Res.* **2014,** *2*, 1-4.
3. Afif, A.; Radenahmad, N.; Cheok, Q.; Shams, S.; Kim, J. H.; Azad, A. K., Ammonia-Fed Fuel Cells: A Comprehensive Review. *Renew. Sust. Energ. Rev.* **2016,** *60*, 822-835.
4. Klerke, A.; Christensen, C. H.; Nørskov, J. K.; Vegge, T., Ammonia for Hydrogen Storage: Challenges and Opportunities. *J. Mater. Chem.* **2008,** *18*, 2304-2310.
5. Adli, N. M.; Zhang, H.; Mukherjee, S.; Wu, G., Review—Ammonia Oxidation Electrocatalysis for Hydrogen Generation and Fuel Cells. *J. Electrochem. Soc.* **2018,** *165*, J3130-J3147.
6. Schüth, F.; Palkovits, R.; Schlögl, R.; Su, D. S., Ammonia as a Possible Element in an Energy Infrastructure: Catalysts for Ammonia Decomposition. *Energy Environ. Sci.* **2012,** *5*, 6278-6289.
7. Dunn, P. L.; Cook, B. J.; Johnson, S. I.; Appel, A. M.; Bullock, R. M., Oxidation of Ammonia with Molecular Complexes. *J. Am. Chem. Soc.* **2020,** *142*, 17845-17858.
8. Lamb, K. E.; Dolan, M. D.; Kennedy, D. F., Ammonia for Hydrogen Storage; A Review of Catalytic Ammonia Decomposition and Hydrogen Separation and Purification. *Int. J. Hydrog. Energy* **2019,** *44*, 3580-3593.
9. Habibzadeh, F.; Miller, S. L.; Hamann, T. W.; Smith, M. R. Homogeneous Electrocatalytic Oxidation of Ammonia to N_2 Under Mild Conditions. *Proc. Natl. Acad. Sci. U.S.A.* **2019,** *116*, 2849-2853.
10. Bhattacharya, P.; Heiden, Z. M.; Chambers, G. M.; Johnson, S. I.; Bullock, R. M.; Mock, M. T., Catalytic Ammonia Oxidation to Dinitrogen by Hydrogen Atom Abstraction. *Angew. Chem. Int. Ed.* **2019,** *58*, 11618-11624.
11. Dunn, P. L.; Johnson, S. I.; Kaminsky, W.; Bullock, R. M., Diversion of Catalytic C–N Bond Formation to Catalytic Oxidation of NH_3 through Modification of the Hydrogen Atom Abstractor. *J. Am. Chem. Soc.* **2020,** *142*, 3361-3365.
12. Zott, M. D.; Garrido-Barros, P.; Peters, J. C., Electrocatalytic Ammonia Oxidation Mediated by a Polypyridyl Iron Catalyst. *ACS Catal.* **2019,** *9*, 10101-10108.
13. Nakajima, K.; Toda, H.; Sakata, K.; Nishibayashi, Y., Ruthenium-Catalysed Oxidative Conversion of Ammonia into Dinitrogen. *Nat. Chem.* **2019,** *11*, 702-709.
14. Zott, M. D.; Peters, J. C., Enhanced Ammonia Oxidation Catalysis by a Low-Spin Iron Complex Featuring *Cis* Coordination Sites. *J. Am. Chem. Soc.* **2021,** *143*, 7612-7616.
15. Li, Y.; Chen, J.-Y.; Miao, Q.; Yu, X.; Feng, L.; Liao, R.-Z.; Ye, S.; Tung, C.-H.; Wang, W., A Parent Iron Amido Complex in Catalysis of Ammonia Oxidation. *J. Am. Chem. Soc.* **2022,** *144*, 4365-4375.
16. Trenerry, M. J.; Wallen, C. M.; Brown, T. R.; Park, S. V.; Berry, J. F., Spontaneous N_2 Formation by a Diruthenium Complex Enables Electrocatalytic and Aerobic Oxidation of Ammonia. *Nat. Chem.* **2021,** *13*, 1221-1227.
17. Zhang, H.; Wang, Y.; Wu, Z.; Leung, D. Y. C., An Ammonia Electrolytic Cell with NiCu/C as Anode Catalyst for Hydrogen Production. *Energy Procedia* **2017,** *142*, 1539-1544.
18. Muthuvel, M.; Botte, G. G., Trends in Ammonia Electrolysis. In *Modern Aspects of Electrochemistry, No. 45*, White, R. E., Ed. Springer New York: New York, NY, 2009; pp 207-245.
19. Concepcion, J. J.; Jurss, J. W.; Templeton, J. L.; Meyer, T. J., One Site is Enough. Catalytic Water Oxidation by $[Ru(tpy)(bpm)(OH_2)]^{2+}$ and $[Ru(tpy)(bpz)(OH_2)]^{2+}$. *J. Am. Chem. Soc.* **2008,** *130*, 16462-16463.
20. Duan, L.; Bozoglian, F.; Mandal, S.; Stewart, B.; Privalov, T.; Llobet, A.; Sun, L., A Molecular Ruthenium Catalyst with Water-Oxidation Activity Comparable to that of Photosystem II. *Nat. Chem.* **2012,** *4*, 418-423.
21. Blakemore, J. D.; Crabtree, R. H.; Brudvig, G. W., Molecular Catalysts for Water Oxidation. *Chem. Rev.* **2015,** *115*, 12974-13005.
22. Najafian, A.; Cundari, T. R., Computational Mechanistic Study of Electro-Oxidation of Ammonia to N_2 by Homogenous Ruthenium and Iron Complexes. *J. Phys. Chem. A* **2019,** *123*, 7973-7982.
23. Holub, J.; Vereshchuk, N.; Sánchez-Baygual, F.-J.; Gil-Sepulcre, M.; Benet-Buchholz, J.; Llobet, A., Synthesis, Structure, and Ammonia Oxidation Catalytic Activity of Ru-NH_3 Complexes Containing Multidentate Polypyridyl Ligands. *Inorg. Chem.* **2021,** *60*, 13929-13940.
24. Raghibi Boroujeni, M. G., C.; Bertke, J. A.; Warren, T. H. Chemical and Electrocatalytic Ammonia Oxidation by Ferrocene. *ChemRxiv* **2019**, DOI: 10.26434/chemrxiv.9729635.v1.
25. Scheibel, M. G.; Abbenseth, J.; Kinauer, M.; Heinemann, F. W.; Würtele, C.; de Bruin, B.; Schneider, S., Homolytic N–H Activation of Ammonia: Hydrogen Transfer of Parent Iridium Ammine, Amide, Imide, and Nitride Species. *Inorg. Chem.* **2015,** *54*, 9290-9302.
26. Betley, T. A.; Peters, J. C., A Tetrahedrally Coordinated $L_3Fe{-}N_x$ Platform that Accommodates Terminal Nitride (Fe^{IV}:N) and Dinitrogen ($Fe^{I}{-}N_2{-}Fe^{I}$) Ligands. *J. Am. Chem. Soc.* **2004,** *126*, 6252-6254.
27. Coia, G. M.; Devenney, M.; White, P. S.; Meyer, T. J.; Wink, D. A., Osmium Hydrazido and Dinitrogen Complexes. *Inorg. Chem.* **1997,** *36*, 2341-2351.

28. Gu, N. X.; Oyala, P. H.; Peters, J. C., Hydrazine Formation via Coupling of a Nickel(III)–NH_2 Radical. *Angew. Chem. Int. Ed.* **2021,** *60*, 4009-4013.
29. Gephart Iii, R. T.; Huang, D. L.; Aguila, M. J. B.; Schmidt, G.; Shahu, A.; Warren, T. H., Catalytic C–H Amination with Aromatic Amines. *Angew. Chem. Int. Ed.* **2012,** *51*, 6488-6492.
30. Wiese, S.; Badiei, Y. M.; Gephart, R. T.; Mossin, S.; Varonka, M. S.; Melzer, M. M.; Meyer, K.; Cundari, T. R.; Warren, T. H., Catalytic C–H Amination with Unactivated Amines through Copper(II) Amides. *Angew. Chem. Int. Ed.* **2010,** *49*, 8850-8855.
31. Jang, E. S.; McMullin, C. L.; Käß, M.; Meyer, K.; Cundari, T. R.; Warren, T. H., Copper(II) Anilides in sp^3 C–H Amination. *J. Am. Chem. Soc.* **2014,** *136*, 10930-10940.
32. Jayasooriya, I. U.; Bakhoda, A.; Palmer, R.; Ng, K.; Khachemoune, N. L.; Bertke, J. A.; Warren, T. H., Copper(II) Ketimides in sp^3 C–H Amination. *Chem. Sci.* **2021,** *12*, 15733-15738.
33. Ryan, M. C.; Kim, Y. J.; Gerken, J. B.; Wang, F.; Aristov, M. M.; Martinelli, J. R.; Stahl, S. S., Mechanistic Insights into Copper-Catalyzed Aerobic Oxidative Coupling of N–N bonds. *Chem. Sci.* **2020,** *11*, 1170-1175.
34. Wang, F.; Gerken, J. B.; Bates, D. M.; Kim, Y. J.; Stahl, S. S., Electrochemical Strategy for Hydrazine Synthesis: Development and Overpotential Analysis of Methods for Oxidative N–N Coupling of an Ammonia Surrogate. *J. Am. Chem. Soc.* **2020,** *142*, 12349-12356.
35. Carey, D. T.; Cope-Eatough, E. K.; Vilaplana-Mafé, E.; Mair, F. S.; Pritchard, R. G.; Warren, J. E.; Woods, R. J., Structures and Reactions of Monomeric and Dimeric Lithium Diazapentadienyl Complexes with Electrophiles: Synthesis of α-C,C′-dialkyl-β-diimines, and Dissolution-Reversible Synthesis of an α-Alkoxylithium-β-diimine. *Dalton Trans.* **2003,** 1083-1093.
36. Salvador, T. K.; Arnett, C. H.; Kundu, S.; Sapiezynski, N. G.; Bertke, J. A.; Raghibi Boroujeni, M.; Warren, T. H., Copper Catalyzed sp^3 C–H Etherification with Acyl Protected Phenols. *J. Am. Chem. Soc.* **2016,** *138*, 16580-16583.
37. Rountree, E. S.; McCarthy, B. D.; Eisenhart, T. T.; Dempsey, J. L., Evaluation of Homogeneous Electrocatalysts by Cyclic Voltammetry. *Inorg. Chem.* **2014,** *53*, 9983-10002.
38. Roy, S.; Sharma, B.; Pécaut, J.; Simon, P.; Fontecave, M.; Tran, P. D.; Derat, E.; Artero, V., Molecular Cobalt Complexes with Pendant Amines for Selective Electrocatalytic Reduction of Carbon Dioxide to Formic Acid. *J. Am. Chem. Soc.* **2017,** *139*, 3685-3696.
39. Costentin, C.; Drouet, S.; Robert, M.; Savéant, J.-M., Turnover Numbers, Turnover Frequencies, and Overpotential in Molecular Catalysis of Electrochemical Reactions. Cyclic Voltammetry and Preparative-Scale Electrolysis. *J. Am. Chem. Soc.* **2012,** *134*, 11235-11242.
40. Siu, J. C.; Sauer, G. S.; Saha, A.; Macey, R. L.; Fu, N.; Chauviré, T.; Lancaster, K. M.; Lin, S., Electrochemical Azidooxygenation of Alkenes Mediated by a TEMPO–N_3 Charge-Transfer Complex. *J. Am. Chem. Soc.* **2018,** *140*, 12511-12520.
41. Hathaway, B. J.; Tomlinson, A. A. G., Copper(II) Ammonia Complexes. *Coord. Chem. Rev.* **1970,** *5*, 1-43.
42. Constable, E. C.; Housecroft, C. E., Coordination Chemistry: The Scientific Legacy of Alfred Werner. *Chem. Soc. Rev.* **2013,** *42*, 1429-1439.
43. Libavius, A. *D. O. M. A. Commentationum Metallicarum Libri Quatuor de Natura Metallorum, Mercurio Philosophorum, Azotho, et Lapide seu tinctura physicorum conficienda e` Rerum Natura, Experientia, et Autorum præstantium fide*, Frankfurt, **1597**.

TOC Graphic

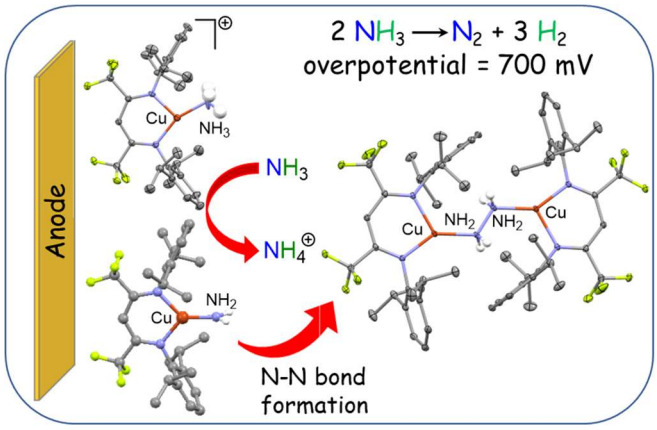
2 NH3 → N2 + 3 H2
overpotential = 700 mV
Anode
Cu
NH3
NH3
NH4
NH2
Cu
Cu
NH2
NH2
Cu
N-N bond
formation